

Influences of Shear Angles on Microstructures and Compression Properties of AZ31 Mg Alloy Prepared by Extrusion-Shear Process

Feng Jingkai^{1,2}, Zhang Dingfei^{1,2}, Yuan Yuan^{1,2}, Zhao Yang^{1,2}, Chen Xia^{1,2}, Chai Sen-sen⁵, Hu Hongjun⁴, Jiang Bin^{1,2}, Pan Fusheng^{2,3}

¹ College of Materials Science and Engineering, Chongqing University, Chongqing 400045, China; ² National Engineering Research Center for Magnesium Alloys, Chongqing University, Chongqing 400044, China; ³ Chongqing Academy of Science and Technology, Chongqing 401123, China; ⁴ College of Materials Science and Engineering, Chongqing University of Technology, Chongqing 400054, China; ⁵ School of Metallurgy and Materials Engineering, Chongqing University of Science and Technology, Chongqing 401331, China

Abstract: AZ31 rods were prepared by the extrusion-shear (ES) process with different shearing angles (150°, 135° and 120°), including direct extrusion process and subsequent shearing process. Microstructure evolution of AZ31 alloys with bimodal grains was investigated by optical microscopy (OM), scanning electron microscopy and electron back scattered diffraction (EBSD), etc. The results show that proportion of the large grain areas increases with the increase of strain. Bimodal-grained structures are observed by OM, and the narrow coarse grains are surrounded by the fine grains. The pole figures show that the texture changes with different shearing angles of the ES mould. Both the yield strengths and the peak strengths increase with decrease of the shearing angles gradually. As the shearing strain increases, the proportion of large grains increases while the size of small grains increases because both the deformation and the dynamic recrystallization fractions increase with the decrease of shearing angles.

Key words: extrusion-shear (ES) process; magnesium alloy; bimodal grain; EBSD; compression

Magnesium alloys, as the lightest commercial structural metallic materials, have great potential in the field of aerospace and automobile industry. Their advantages of magnesium alloys such as high specific strength, high specific rigidity, good damping capacity and rich resources have attracted researchers' attention^[1,2]. However, magnesium alloy generally exhibits poor deformation capacity at room temperature due to their hexagonal close-packed (hcp) crystal structure. Besides, the strength of magnesium alloy is still not comparable to that of high strength steel or even high strength aluminum alloy. So the development of magnesium alloy is not as fast as it should have been^[3-5].

Severe plastic deformation (SPD) techniques have shown great advantages in improving the strength and ductility of

magnesium alloys. Typical ultra-fine grained (UFG) structure can be obtained for magnesium alloys and the grain sizes are less than 1 μm . It is well known that fine grain size is beneficial to improve the strength and ductility of metallic materials simultaneously. Therefore, SPD methods have been used extensively for grain refinements and formability improvement of magnesium alloys^[6]. Over the last decade, several SPD methods have been proposed, such as cyclic expansion-extrusion (CEE)^[7], twist extrusion (TE)^[8], equal-channel angular pressing (ECAP) and high-pressure torsion (HPT)^[6], etc.

Though the ultra-fine grained magnesium alloys fabricated by SPD exhibit high yield stress based on Hall-Petch relationship, their ductility and toughness are still poor^[9]. In

Received date: February 18, 2020

Foundation item: National Key Research and Development Program of China (2016YFB0301101); National Natural Science Foundation of China (51571040, U1764253, 51531002)

Corresponding author: Zhang Dingfei, Ph. D., Professor, College of Materials Science and Engineering, Chongqing University, Chongqing 400045, P. R. China, Tel: 0086-23-65112491, E-mail: zhangdingfei@cqu.edu.cn

Copyright © 2021, Northwest Institute for Nonferrous Metal Research. Published by Science Press. All rights reserved.

order to improve the ductility and toughness of the fine-grain structure, an idea of bimodal structure which includes fine grain (FG) and coarse grain (CG) structures has been proposed^[10]. The purpose is to increase ductility, but the strength may drop. Some studies have shown that a good combination of strength and ductility can be obtained by introducing bimodal structures into magnesium alloys^[9,11,12]. The research of the nanostructured metals with bimodal grains was firstly published by Tellkamp^[13] et al and Wang^[14] et al. Their works indicated that high strength and good ductility can be obtained simultaneously in the UFG copper alloys. Shekhar^[15] et al used the SPD method to obtain the multi-modal grain size in the copper alloy, and it was found that the ductility of the copper with multi-modal grain size is obviously higher than that of the copper alloy with coarse grains. Many theoretical studies have analyzed the mechanical performance of the bimodal-grained alloys, which is relevant to the grain size and volume fraction of CG^[16].

Owing to the excellent mechanical properties of bimodal-grained materials, more and more attention has been paid to the relevant experimental and modeling research. However, the influences of bimodal grains on the mechanical properties of magnesium alloys have not been revealed distinctly.

The process to prepare magnesium alloy rods includes two consecutive processes (extrusion process and subsequent shearing process, ES), which is put forward by Hu and Zhang^[17] et al. In this study, the commercial AZ31 magnesium alloy was prepared by ES process. In addition, three different shearing angles of ES mould were adopted, which would result in different strains and CG area ratios in the rods. Then the compression properties of the rods were analyzed by the microstructure distribution and the EBSD data of the compression process. The influences of the bimodal-grain structure on material properties were discussed.

1 Experiment

The as-received rods were extruded by ES process, and the diagrammatic sketch of ES mould is shown in Fig.1. It consists

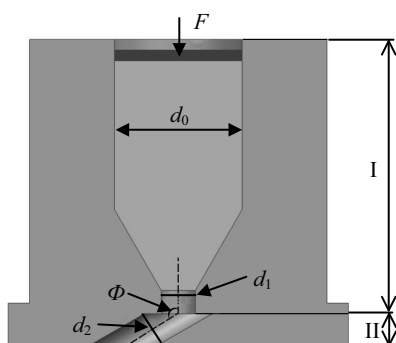


Fig.1 Schematic diagram of ES mould

of two sections: (I) a conical section which includes upsetting zone and sizing zone; (II) a sloping channel section. In the conical section, the rod diameter can be reduced from 60 mm to 16 mm, and extrusion ratio is 14. Different shear angles Φ are controlled by the shearing part, which are equal to 150°, 135° and 120°.

The material used in this study was the commercial AZ31 magnesium alloy with chemical composition of Mg-3Al-1Zn-0.6Mn (wt%). A very low fraction of Mg17Al12 particles existed in the initial microstructure. The as-cast billets were machined into round billets which were 60 mm in diameter and 70 mm in length before extrusion. Then the billets and the ES mould were heated to 623 K and insulated. Subsequently, the ES process started. The ES was conducted at 593±5 K by a hydraulic press of 200-ton capacity with an extrusion speed of 5 mm·s⁻¹. Finally, three rods were extruded by ES mould with different shear angles.

The microstructures of the cross-section which were perpendicular to the extrusion direction (ED) were characterized by optical microscope (OM). The samples were ground, polished and etched in acetic picral including 2 mL acetic acid, 10 mL ethanol and 2 g picric acid. Grain size was measured by Image-pro Plus software. Crystallographic texture measurements were conducted by X-ray diffraction in the reflection geometry with a 3-axis goniometer and Cu K α radiation.

The comprehensive mechanical properties were determined by micro-hardness tests, tensile tests and compression tests. The micro-hardness of the samples was measured by an HXS-1000AY Vickers hardness tester with a load of 200 g and testing time of 15 s. At least 15 points of each sample were tested, and the average micro-hardness was obtained. The compression samples were machined into rectangle with the size of 7 mm×7 mm×10 mm.

2 Results

2.1 Microstructures

Fig.2 presents the OM images of the samples after ES process with different shear angles. It can be observed that three samples have the bimodal-grained structure, and the narrow CG areas are surrounded by the continuous FG. 800~1000 grains from at least three OM images of each sample are selected randomly to calculate the grain sizes. The boundary of coarse grains and fine grains is defined according to the distribution maps. And the boundary line used to estimate the area ratio of coarse grains is shown in Fig.3.

In Fig.3a~3c, the grains of different sizes are approximately normally distributed in the range of grain size greater than 10 μ m and smaller than 10 μ m. Therefore, 10 μ m is selected as the grain size boundary standard for FG and CG in this research. There are obvious extrusion flow lines along the ED, and there are some fine dynamic recrystallized grains among deformed coarse grains. During the ES process, the strain

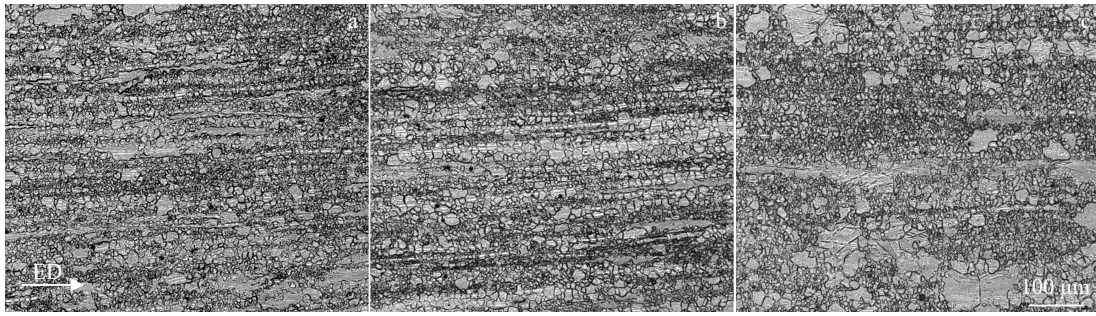


Fig.2 OM images of samples prepared by ES process with different shear angles Φ : (a) 150°, (b) 135°, and (c) 120°

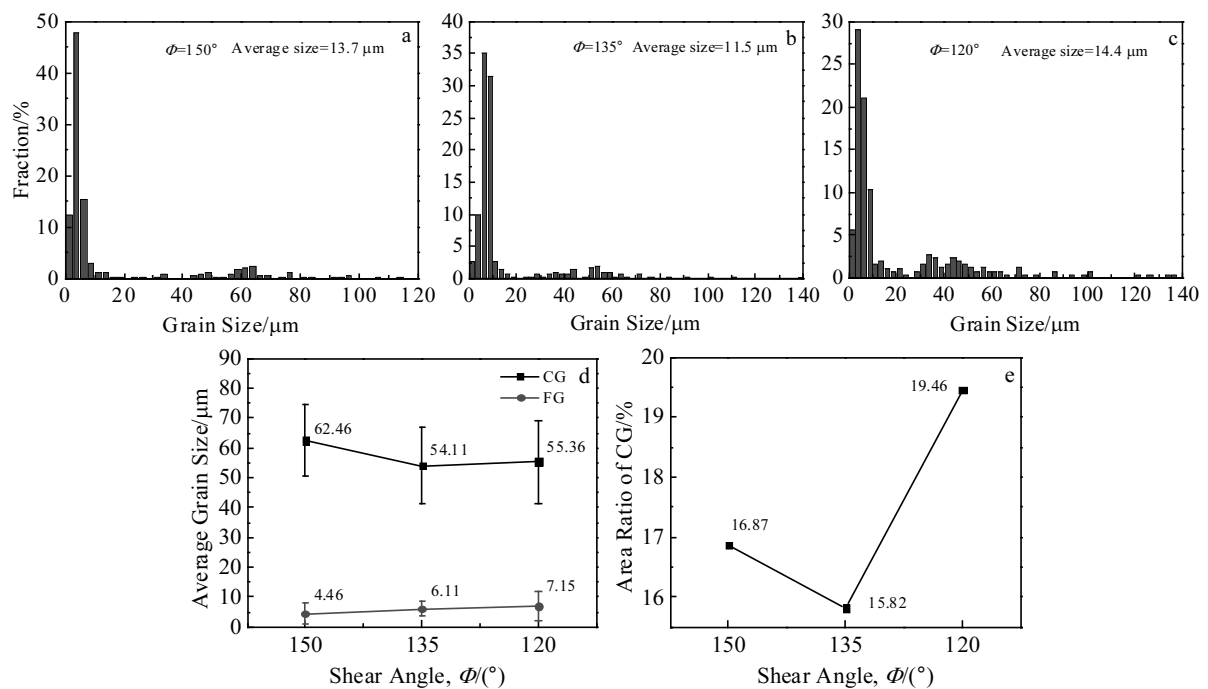


Fig.3 Grain sizes of samples prepared by ES process with 150° (a), 135° (b), and 120° (c) in shear angle; average grain size of coarse grain (CG) and fine grain (FG) with different shear angles (d); area ratio of coarse grain (CG) with different shear angles (e)

increases with decrease of the shearing angles of ES mould gradually, the dynamic recrystallization becomes complete progressively, and the grains begin to grow. The elongated CG is replaced by the FG gradually (Fig.2b). When shear angle is 120°, the uniform grains begin to grow (Fig.2c). Besides, the average grain size of the CG does not decrease with shear angle monotonically. When the shear angle is 120°, the average grain size of the CG increases slightly (Fig.3d). The average grain size of FG increases slightly with the decrease of shear angles. The evolution law of grain size is consistent with the observation of the OM images. Fig.3e shows the CG area ratio. As the shear angle reduces, the variation tendency of CG area ratio is similar to the change of the average size of CG. The order of the proportion of CG areas is as follows:

120° (19.46%) > 150° (16.87%) > 135° (15.82%).

2.2 Texture

The pole figures illustrate the crystal orientation (*c*-axis) of the grains. The (0002) pole figures which are perpendicular to the rod axis for the ES-processed materials are shown in Fig.4. The pole figures demonstrate that textures change with different shearing angles of the ES mould. (0002) pole of magnesium alloy prepared by direct extrusion is shown in Fig.4a. The different colors indicate the texture intensities, and the maximum intensity of the macrotexture is 9.7. It can be seen that there are {0002} basal textures in AZ31 magnesium alloy fabricated by direct extrusion without shear angle. The texture is a symmetrical ring, and base plane (0001) is parallel to ED substantially.

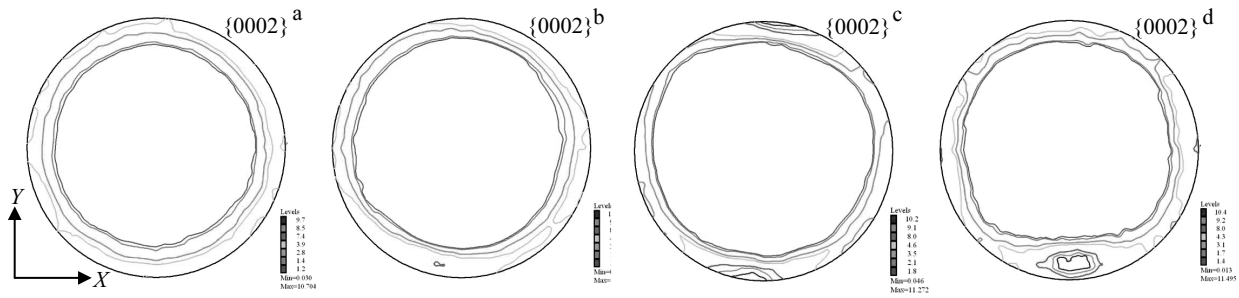


Fig.4 Pole figures of the samples prepared by ES process with different shear angles: (a) without shear process, (b) 150°, (c) 135°, and (d) 120°

Grain orientations of AZ31 magnesium alloy change during the ES process, leading to the preferred orientation of the crystal grains, and then textures are produced. Fig.4b~4d are the (0002) pole figures of magnesium alloy fabricated by ES mould with shear angle of 150°, 135° and 120°, respectively.

Fig.4b shows the macrotexture of the extruded rod with extrusion temperature of 315 °C and shear angle of 150° of ES mould. The texture is a typical (10 $\bar{1}$ 0) texture, but the strength of which improves significantly, indicating that the additional shear is beneficial to the formation of basal plane (0002) which is parallel to the ED. Fig.4c shows the macrotexture of the extruded rod prepared by ES mould with shear angle of 135° and extrusion temperature of 315 °C, and the texture intensity is still high.

2.3 Mechanical properties

The micro-hardnesses of samples are shown in Fig.5a, which depicts hardness varying with change of shearing angles. The change trend of micro-hardness is exactly opposite to that of the area ratio of CG. The order of hardness HV is as follows: 135° (601 MPa)>120° (595 MPa)>150° (572 MPa). The average micro-hardness with shear angle of 135° and 120° is higher than that with shear angle of 150°, and the difference is slight.

The stress-strain curves of samples under different compression conditions at the room temperature are presented in Fig.5b, and compression mechanical properties of samples are shown in Table 1. The compression curves are all concave, and the shape of the stress-strain curve is characteristic of extruded magnesium alloys including extension twinning^[18].

From the results in Table 1, the order of compression yield strength is: 120° (134 MPa)>135° (129 MPa)>150° (124 MPa); the order of ultimate compression strength is: 120° (473 MPa)>135° (436 MPa)>150° (384 MPa).

Both the yield strength and the peak strength increase with dropping of the shear angles gradually, which is different from the change trend of previous microstructure and micro-hardness. CG proportion of the samples fabricated by ES mould with shear angle of 120° is the largest, and the compression strength is the highest, which is different from the rule of Hall-Petch.

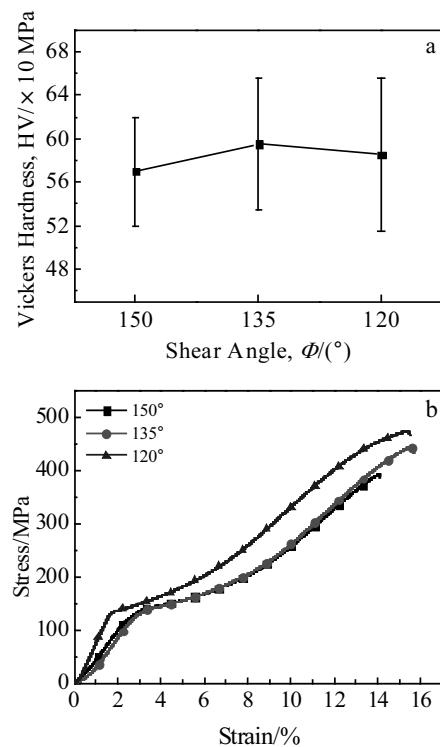


Fig.5 Vickers hardness HV (a) and stress-strain curves (b) of samples with different shear angles

Table 1 Compression properties of samples fabricated by ES process with different shear angles (MPa)

Shearing angle	150°	135°	120°
Compression yield strength	124	129	134
Ultimate compression strength	384	436	473

2.4 Microstructure after 4% compression deformation

Fig.6 shows the EBSD data of the extruded rods prepared by ES process with different shear angles, which includes the IPF figures with and without 4% compression deformation. In the IPF map, high angle grain boundaries (HAGBs) are presented by black lines, and low angle grain boundaries (LAGBs) are presented by white lines. LAGBs are presented by gray

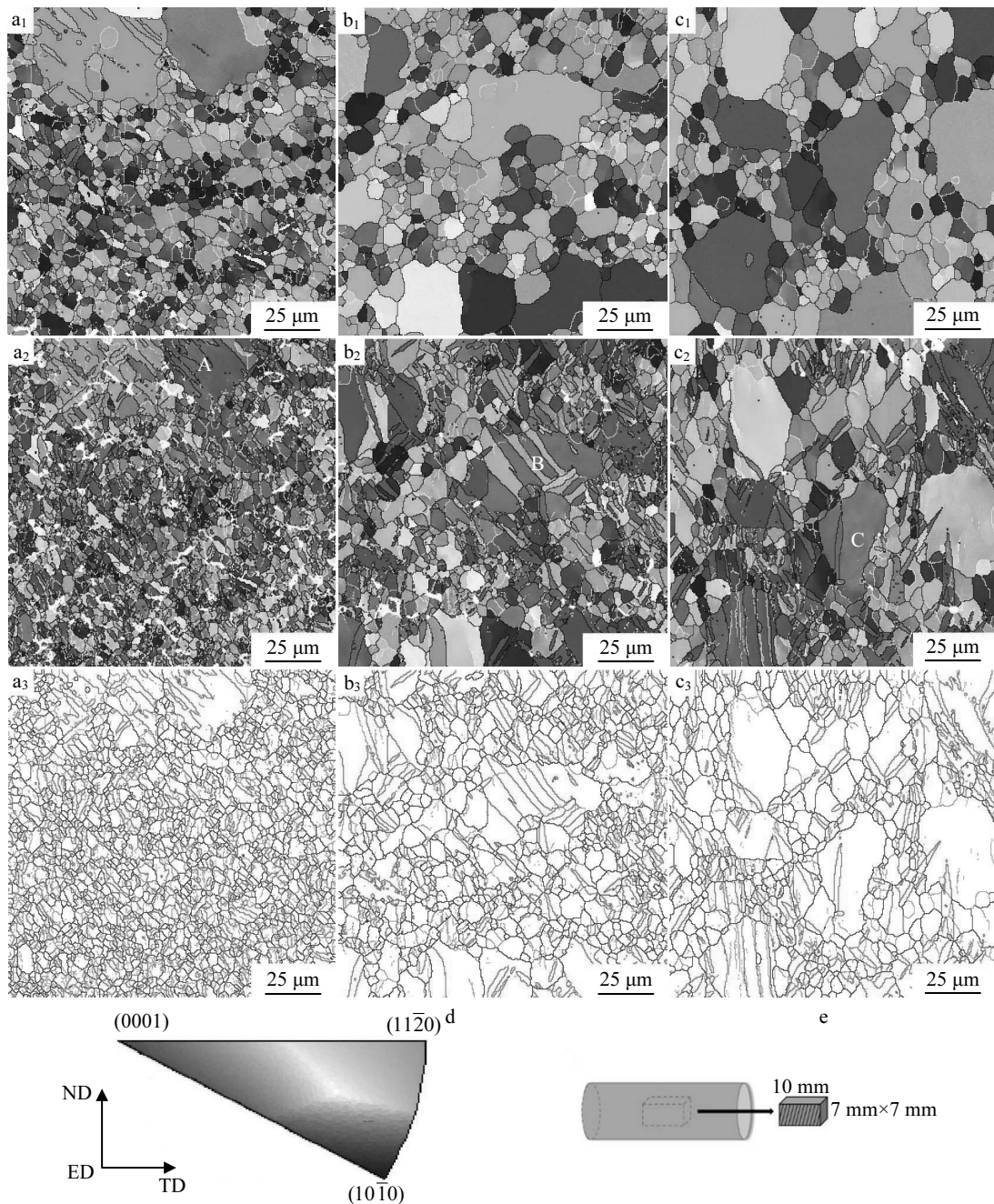


Fig.6 Orientation imaging maps for samples with shear angle of 150° (a_1 ~ a_3), 135° (b_1 ~ b_3), and 120° (c_1 ~ c_3): (a_1 , b_1 , c_1) initial sample, (a_2 , b_2 , c_2) samples after 4% compression deformation, and (a_3 , b_3 , c_3) grain boundary distribution map of sample after compression; notation of the sample coordinate convention (d); sampling point (e)

lines and $\{10\bar{1}2\}$ tensile twin boundaries are presented by red lines. The notations of the sample coordinate convention are shown in Fig.6d. The samples are taken from the site labeled in Fig.6e.

It can be seen from Fig.6a₁, 6b₁ and 6c₁ that the microstructure characteristics are consistent with the OM images which exhibit typical bimodal grains structures. As the shear strains increase, the proportion of large grains increase while

the size of small grains increases as well because both the deformation and the dynamic recrystallization fraction increase with the decrease of shear angle. It can also be proved by the recrystallization distribution diagram in red regions, substructure in yellow regions, and recrystallized structure in blue regions in Fig.7.

The proportion of the blue region increases with dropping of the shear angle significantly, and the large grains are

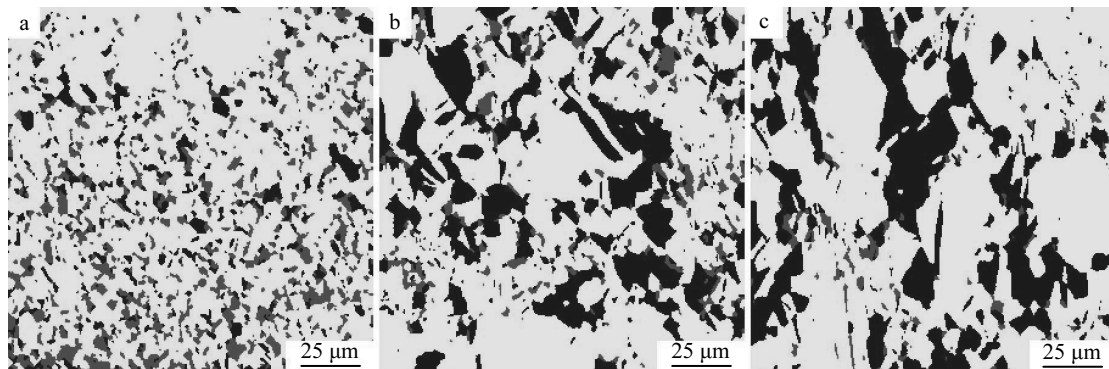


Fig.7 Dynamic recrystallization maps of sample with shear angle of 150° (a), 135° (b), and 120° (c) for EBSD tests

situated in the blue region, which indicates that the coarse grains are elongated during the deformation process when the shear angle increases. Recrystallized grains grow coarser when the shear angle of ES mould is smaller.

There are many red twins between the original blue and green grains in Fig.6a₂, 6b₂, and 6c₂. It can be seen that the grain misorientation angle is about 86° in Fig.8, indicating that most of the twins are $\{10\bar{1}2\}$ tensile twins. Because the textures of the magnesium alloy fabricated by ES process are fiber texture which are beneficial for the generation of tensile twins when forces are applied along the ED^[18]. Fig.6a₃, 6b₃ and 6c₃ show some distinct peaks ($86^\circ <1\bar{2}10>$) corresponding to $\{10\bar{1}2\}$ twins, and the proportion of twins is 16.4% (150°), 18.5% (135°) and 20.8% (120°). The number of twins also varies with the shear angle linearly, because the coarse grains are more favorable for twinning^[19].

The pole figures of ES-processed magnesium alloy before and after 4% compression deformation are shown in Fig.9. The micro pole figures before deformation are similar to the macro pole diagrams. It is found that the basal planes (0001) of most grains are parallel to the extrusion direction in Fig.9a₁, 9b₁ and 9c₁. Furthermore, as the shear angles decrease, the (0002) planes deflect slightly. From the $(10\bar{1}0)$ pole figures, it is found that the deflection causes diffusion of grain

orientations after initial extrusion, resulting in the decrease of texture intensity.

The 4% compression-deformed sample shows a large deflection of $\{10\bar{1}2\}$, and the original grains show deflection angle at 86.3°. In addition, many (0002) basal planes are perpendicular to the ED in Fig.9a₂, 9b₂ and 9c₂ approximately. The texture intensities are lower than those of the initial textures of magnesium alloy before compression deformation.

3 Discussion

Continuous dynamic recrystallization coexists with discontinuous dynamic recrystallization during the hot working process of the AZ31 magnesium alloy^[20,21]. The recrystallization nucleation points are usually near the grain boundary or twin boundary due to the high density of dislocations among the grain boundaries in the areas controlled by discontinuous dynamic recrystallization^[22].

If the size of the initial grains differs from that of the recrystallized grains, bimodal-grained structure forms^[23]. At the same time, the distinction between the nucleation grains and growth grains of continuous dynamic recrystallization is not obvious. The results show that ES processes promote formation of bimodal-grained microstructures with different CG area ratios.

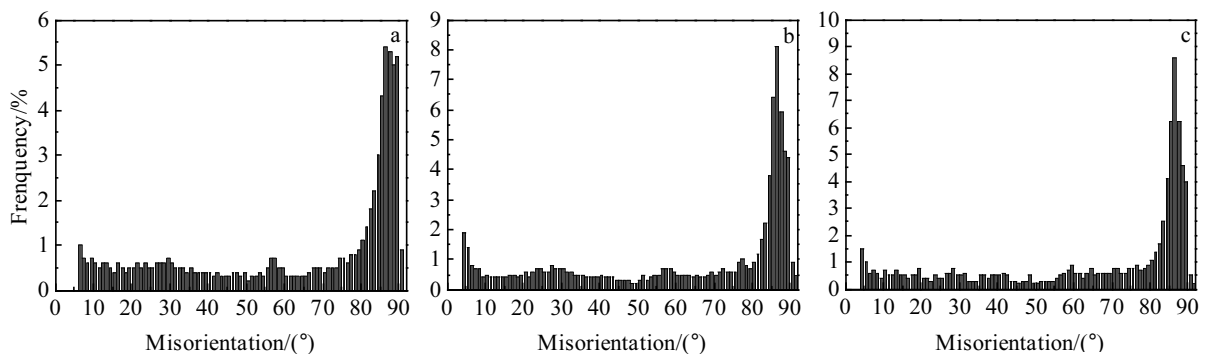


Fig.8 Misorientation of grains of sample with different shear angles: (a) 150°, (b) 135°, and (c) 120°

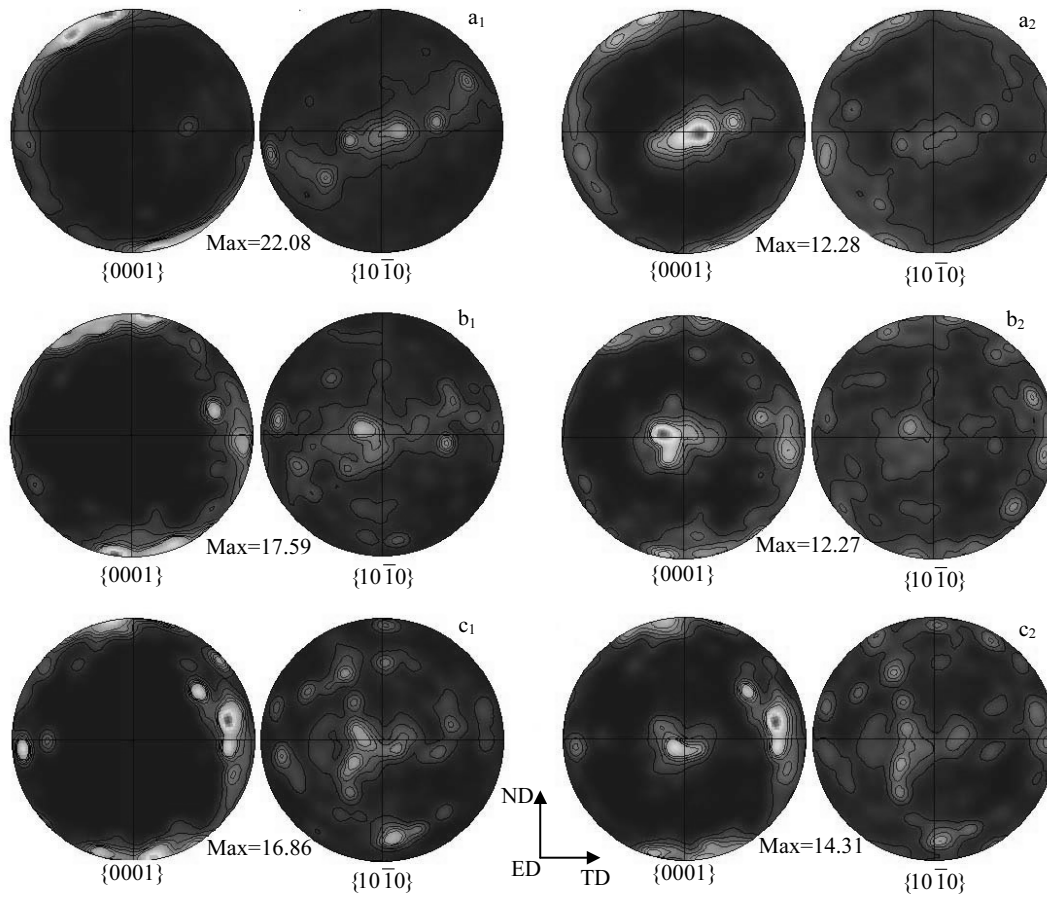


Fig.9 Pole figures for samples before (a₁, b₁, c₁) and after (a₂, b₂, c₂) 4% compression deformation with shear angle of 150° (a₁, a₂), 135° (b₁, b₂), and 120° (c₁, c₂)

The grain boundaries of magnesium alloys play a fundamental role in determining properties, such as strength, work hardening and mechanical shocks, etc^[24]. A reduction in the grain size can enhance the yield strength, as the Hall-Petch relationship shows^[25]:

$$\sigma_y = \sigma_0 + kd^{-1/2} \quad (1)$$

where σ_y is the yield strength, σ_0 is the friction stress for dislocation movement, k is the strength coefficient for the normal stress, and d is the grain size. This formula is also available for the tensile yield and compression yield. According to Yu's research^[26], the tensile and compressive yield strengths increase linearly with the increase of $d^{-1/2}$. However, the compressive yield strength of the bimodal-grained samples obtained in this experiment does not conform to this rule (Table 1). Therefore, the average grain size is not the key factor affecting the bimodal-grained samples. Based on the macroscopic textures, it is known that although the shear angle causes a slight deflection of the texture, the overall orientation is still hard on the external force along the ED, and the effects on performance are not great.

It is found that the change in the yield strength of the compression test is opposite to the ratio of the CG area. CG is

more conducive to the formation of twins. It is speculated that twins may have a certain impact on the yield strength. Garcés^[27] found that the compressive behavior of the bimodal-grain structure alloy is controlled mostly by extension twinning. Fig.6a₁, 6b₁, and 6c₁ show the IPF maps of sample before compression deformation and the SF is calculated by Eq.(2)^[9], which reflects the $\{10\bar{1}2\}$ twinning activity.

$$SF = \cos\lambda \cdot \cos\varphi \quad (2)$$

where λ is the angle between the load direction and the normal of twin plane, and φ is the angle between the normal of twin plane and shear direction. The SF values of the $\{10\bar{1}2\}$ $[10\bar{1}\bar{1}]$ tensile twins obtained from magnesium alloy fabricated by ES process with shear angle of 150°, 135° and 120° are 0.39, 0.41 and 0.44, respectively. The higher the SF value, the lower the stress value required to activate the twin $\{10\bar{1}2\}$.

When the shear angle is 120°, the ratio of large grain area is 19.5%, and the SF value is also the highest (0.44). Similarly, the proportion of twins (20.8%) is the highest for the ES-processed magnesium alloy after 4% compression deformation with shear angle of 120°.

Three coarse grains containing twins are selected from Fig.6a₂, 6b₂, and 6c₂ (Fig.10). In contrast to Fig.6a₁, 6b₁, and

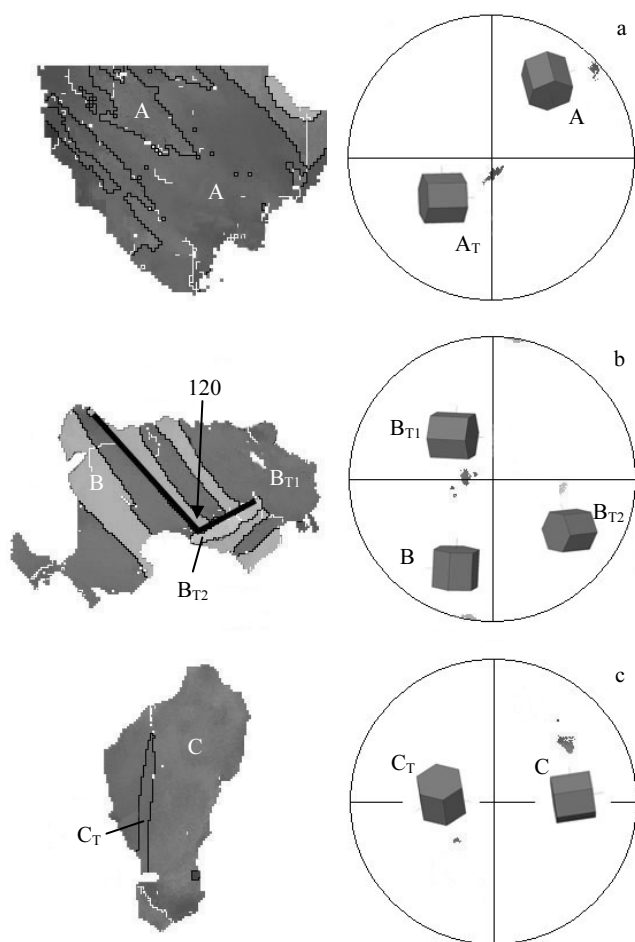


Fig.10 Twin in coarse grains of ES-processed magnesium alloy after 4% compression with different shear angles in Fig.6a₂, 6b₂, and 6c₂: (a) 150°, (b) 135°, and (c) 120°

6c₁, the original crystal grains are marked as A, B, and C, and the twin crystals are marked as A_T, B_T and C_T. These are represented in (0001) pole figures schematically. The *c*-axis of the initial grain is perpendicular to the ED approximately, while there is a deflection of 86.3° in the twin variant along the $[1\bar{2}10]$ axis especially. The *c*-axis of the C_T is parallel to the ED approximately. In addition, B grain also produces two different twin variants, B_{T1} and B_{T2}, and there is an angle of ~120° between the two twins. The generation of twins can refine the grains, and the twins of various variants are intertwined with each other. The twin variants can retard the growth and propagation of the twins' effective bimodal grain, thus an obstacle to the dislocation motion forms and the yield strength can increase.

From the compression curves in Fig.5b, the strain hardening rates of sample fabricated by ES process with shear angle of 120° is the highest, and its peak strength is the highest. In addition to the effects of twinning, significant back stress produced by large strain gradient near the interfaces plays an

important role in work hardening for good ductility^[28].

CG domains (soft domains) are constrained by FG domains (hard domains), urging dislocations to pile up and blocking domain interfaces. When there are large strain gradients, the necessary dislocations will be generated to accommodate the strain gradients in grains, and the dislocations accumulate in the boundary, resulting in back stress hardening^[29]. As the tensile strains increase, the source of dislocations in the CG region (soft domain) activates firstly. It has a tendency to start plastic deformation. However, the CG areas are surrounded by fine grains, and the elastic deformation of the fine-grains may suppress dislocation transmission. As a result, the CG is deformed hardly. Therefore, back stress hardening results in high strain hardening rate and high ductility.

4 Conclusions

- 1) The grain boundary size between coarse grain and fine grain is about 10 μm, and the proportions of the large grain areas increase with the increase of strain.
- 2) When the shear angle is 120°, the area ratio of coarse grain is 19.46%. At the same (4%) pre-compression level, the proportion of large grains, and the proportion of twin boundaries increase in the ES AZ31 Mg alloy.
- 3) Microhardness HV and compression strength of ES sample with shear angle of 120° are greater, reaching 595 MPa and 473 MPa, respectively.
- 4) As the shearing strain increases, the proportion of large grains increases while the size of small grains increases because both the deformation and the dynamic recrystallization fractions increase with the decrease of shearing angle.

References

- 1 Chen Q, Shu D Y, Hu C K et al. *Materials Science and Engineering A*[J], 2012, 541: 98
- 2 Barrett C D, Imandoust A, Oppedal A L et al. *Acta Materialia*[J], 2017, 128: 270
- 3 Mordike B L, Ebert T. *Materials Science and Engineering A*[J], 2001, 302(1): 37
- 4 Eddahbi M, Valle J A D, Pérez-Prado M T et al. *Materials Science and Engineering A*[J], 2005, 410-411: 308
- 5 Liu Y, Cai S L, Dai L H. *Materials Science and Engineering A*[J], 2016, 651: 878
- 6 Alizadeh R, Mahmudi R, Pereira P H R et al. *Materials Science and Engineering A*[J], 2017, 682: 577
- 7 Amani S, Faraji G, Abrinia K. *Journal of Manufacturing Processes*[J], 2017, 28: 197
- 8 Mohammed Iqbal U, Senthil Kumar V S. *Materials & Design*[J], 2013, 50: 946
- 9 Li X F, Zhang J, Hou D W et al. *Materials Science and Engineering A*[J], 2018, 729: 466
- 10 Shen M J, Wang X J, Zhang M F et al. *Composites Science and Technology*[J], 2015, 118: 85
- 11 Zhao M C, Hanamura T, Qiu H et al. *Scripta Materialia*[J], 2006,

- 54(6): 1193
- 12 Koch C. *Scripta Materialia*[J], 2003, 49(7): 657
- 13 Tellkamp V L, Lavernia E J, Melmed A. *Metallurgical and Materials Transactions A*[J], 2001, 32(9): 2335
- 14 Wang Y M, Chen M W, Zhou F H et al. *Nature*[J], 2002, 419(6910): 912
- 15 Shekhar S, Cai J, Wang J et al. *Materials Science and Engineering A*[J], 2009, 527(1-2): 187
- 16 Zhu L L, Shi S Q, Lu K et al. *Acta Materialia*[J], 2012, 60(16): 5762
- 17 Hu H J, Liu Y, Zhang D F et al. *Journal of Alloys and Compounds*[J], 2017, 695: 1088
- 18 Barnett M R, Keshavarz Z, Beer A G et al. *Acta Materialia*[J], 2004, 52(17): 5093
- 19 Xin Y C, Zhou X J, Lv L C et al. *Materials Science and Engineering A*[J], 2014, 606: 81
- 20 Yu H H, Xin Y C, Cheng Y et al. *Materials Science and Engineering A*[J], 2017, 700: 695
- 21 Beer A G, Barnett M R. *Metallurgical and Materials Transactions A*[J], 2007, 38(8): 1856
- 22 Wang Q D, Chen Y J, Liu M P et al. *Materials Science and Engineering A*[J], 2010, 527(9): 2265
- 23 Ponge D, Gottstein G. *Acta Materialia*[J], 1998, 46(1): 69
- 24 Yuan W, Panigrahi S K, Su J Q et al. *Scripta Materialia*[J], 2011, 65(11): 994
- 25 Wang Y, Choo H. *Acta Materialia*[J], 2014, 81: 83
- 26 Yu H H, Xin Y C, Wang M Y et al. *Journal of Materials Science & Technology*[J], 2018, 34(2): 248
- 27 Garcés G, Oñorbe E, Gan W et al. *Materials Characterization*[J], 2017, 126: 116
- 28 Esqué-de los Ojos D, Nguyen C T, Orozco-Caballero A et al. *Materials Science and Engineering A*[J], 2018, 729: 37
- 29 He J H, Jin L, Wang F H et al. *Journal of Magnesium and Alloys*[J], 2017, 5(4): 423

剪切角对挤压-剪切法制备 AZ31 镁合金组织和压缩性能的影响

冯靖凯^{1,2}, 张丁非^{1,2}, 袁圆^{1,2}, 赵阳^{1,2}, 陈霞^{1,2}, 柴森森⁵, 胡红军⁴, 蒋斌^{1,2}, 潘复生^{2,3}

(1. 重庆大学 材料科学与工程学院, 重庆 400045)

(2. 重庆大学 国家镁合金材料工程技术研究中心, 重庆 400044)

(3. 重庆市科学技术研究院, 重庆 401123)

(4. 重庆理工大学 材料科学与工程学院, 重庆 400054)

(5. 重庆科技学院 冶金与材料工程学院, 重庆 401331)

摘要: 采用挤压-剪切法 (ES) 在不同剪切角 (150°、135°和 120°) 下制备了 AZ31 棒材。采用 ES 工艺制备的棒材, 包括直接挤压和后续剪切两部分。随后采用光学显微镜、扫描电镜和电子背散射衍射 (EBSD) 等方法研究了具有双峰晶粒结构的 AZ31 镁合金的显微组织演变, 从取向分布图中可清晰的观察到细晶粒包围狭长变形粗晶的混晶结构, 且大晶粒区域的占比会随应变的增加而增大。整体来看, 因为应变量和动态再结晶分数都会随着剪切角的减小而增加, 导致大晶粒的占比增大, 而小晶粒尺寸增加。室温压缩实验中, 随着剪切角的减小, 屈服强度和峰值强度逐渐增大。此外, ES 挤压的基面极图也会随着剪切角度的不同发生变化。

关键词: 挤压-剪切; 镁合金; 混晶; EBSD; 压缩

作者简介: 冯靖凯, 男, 1992 年生, 博士, 重庆大学材料科学与工程学院, 重庆 400045, E-mail: fengjkcqu@163.com